Journal of Solid State Chemistry 181 (2008) 2041–2045

Contents lists available at ScienceDirect

Journal of Solid State Chemistry

journal homepage: www.elsevier.com/locate/jssc

Alpha-particle-induced luminescence of rare-earth-doped Y_2O_3 nanophosphors

Cory D. Cress [a,b], Christopher S. Redino [a], Brian J. Landi [a], Ryne P. Raffaelle [a,b,*]

[a] NanoPower Research Laboratories at the Rochester Institute of Technology, 85 Lomb Memorial Road, Rochester, NY 14623, USA
[b] Microsystems Engineering Program at the Rochester Institute of Technology, Rochester, NY 14623, USA

ARTICLE INFO

Article history:
Received 28 February 2008
Received in revised form
15 April 2008
Accepted 17 April 2008
Available online 3 May 2008

Keywords:
Yttria
Radioluminescence
Radioisotope battery
Rare earth
Nanophosphors
Alpha-particle detection

ABSTRACT

The feasibility of utilizing Y_2O_3:Tb^{3+} and Y_2O_3:Eu^{3+} as radioluminescent nanophosphors under alpha-particle excitation is investigated. Materials synthesized by the urea homogeneous precipitation method were characterized using scanning electron microscopy (SEM), transmission electron microscopy (TEM), and X-ray diffraction (XRD). The XRD analysis of as-produced precipitates and nanophosphors fired at temperatures ranging from 950 to 1100 °C indicated the presence of highly crystalline cubic Y_2O_3 with crystallite sizes of ~40 nm. SEM and TEM analysis revealed that particles with average diameters of ~200 nm and comprised of ~40 nm grains were obtained. High-resolution radioluminescence and photoluminescence spectra were used to investigate the unwanted radioluminescence saturation effects associated with the high ionization rate of alpha-particles. Additionally, the radioluminescence intensity as a function of rare-earth ion dopant concentration is investigated for these materials under alpha-particle excitation. The prospect for utilizing these materials as intermediate absorbers in indirect-conversion radioisotope batteries is discussed.

1. Introduction

The high energy and power density of radioisotopes have motivated research into devices which can convert the nuclear energy into usable electrical power [1–9]. Such radioisotope power devices could have the ability to power portable electronics and autonomous systems for years to decades. In one manifestation of a radioisotope battery, a radioisotope is placed adjacent to a phosphor layer, which absorbs the energy of the incident particles and re-emits the energy in the form of visible light [2]. The light is subsequently absorbed and converted into electricity via a photovoltaic cell. An indirect-conversion radioisotope battery of this type relies on the phosphor layer to shield the photovoltaic cell, to have a high tolerance to ionizing radiation (e.g., alpha, beta, and gamma), and to have a high-radioluminescence (RL) efficiency. Furthermore, the emission wavelength must be properly matched to the spectral response of the photovoltaic cell.

Rare-earth-doped Y_2O_3 is a prime candidate for use as the phosphor layer in an indirect-conversion radioisotope battery. This material system has been widely studied for use in projection television tubes [10], field emission displays [11], and fluorescent lighting applications [12]. It has also been reported to show high photo- and cathodoluminescence efficiency (e.g., ~95% and ~9% for Y_2O_3:Eu^{3+}, respectively) [2]. Like many oxide-based materials, rare-earth-doped Y_2O_3 has a high resilience to ionizing radiation [2]. Synthesis of rare-earth-doped Y_2O_3-based nanophosphors has been accomplished through a variety of techniques including homogeneous precipitation, chemical vapor synthesis, combustion synthesis, and the sol–gel method [11–15]. The wide variety of dopants that can be incorporated allows the material to be tuned to emit in the blue (Tm^{3+}), green (Er^{3+}, Tb^{3+}), or red (Eu^{3+}) regions of the electromagnetic spectrum [10,16]. Additionally, the wide energy bandgap of the Y_2O_3 material system reduces the effects of optical absorption by the host.

For indirect-conversion radioisotope batteries, proper coupling between the radiation source, phosphor, and photovoltaic cell are required to achieve maximum nuclear-to-electrical conversion efficiency. Assuming a planar geometry, the phosphor layer must be of sufficient thickness to absorb most of the incident radiation but must still allow for transmission of the emitted light. Thus, the synthesis of nanocrystalline Y_2O_3 phosphors (nanophosphors) allows for finer control over the thickness and uniformity of deposited films. This control enables the optimal phosphor layer thickness (which balances the competing effects of nuclear energy absorption and light transmission) to be obtained. This work

* Corresponding author at: NanoPower Research Laboratories at the Rochester Institute of Technology, 85 Lomb Memorial Road, Rochester, NY 14623, USA.
E-mail addresses: cory_cress@hotmail.com, cdc2798@rit.edu (C.D. Cress), csr8932@rit.edu (C.S. Redino), bjlsps@rit.edu (B.J. Landi), rprsps@rit.edu (R.P. Raffaelle).

0022-4596/$ - see front matter © 2008 Elsevier Inc. All rights reserved.
doi:10.1016/j.jssc.2008.04.024

examines the feasibility of using rare-earth-doped Y_2O_3 as a radioluminescent nanophosphor under alpha-particle excitation. Specifically, the development of radioluminescent Y_2O_3:Eu^{3+} and Y_2O_3:Tb^{3+} nanophosphors, synthesized using the urea homogeneous precipitation technique, and characterized under optical and alpha-particle excitation is presented.

2. Experimental

An EDTA-assisted urea precipitation technique [14] was employed to synthesize Y_2O_3:RE^{3+} (RE = Eu, Tb) nanoparticles with precise size control. This process is initiated by dissolving 1.4 g of $Y(NO_3)_3 \cdot 6H_2O$ and a stoichiometric amount of $Eu(NO_3)_3 \cdot 5H_2O$ or $Tb(NO_3)_3 \cdot 5H_2O$ in 400 mL of deionized H_2O (18.3 MΩ). To this solution, 9.0 g of urea and 0.12 g of EDTA are added and subsequently heated to 50 °C under mild stirring for complete dissolution. The temperature is raised to ~100 °C and soon after a white precipitate can be observed, which is allowed to evolve for one additional hour. After cooling to room temperature, the solution is filtered using a 0.02 μm anode disk alumina filter, rinsed three times with H_2O, and dried *in vacuo* at 90 °C for 4 h. After drying, a fine white $(Y_{1-x}RE_x)OHCO_3 \cdot H_2O$ powder results; the values of x range from 0.01 to 0.15 for the RE = Eu and 0.001–0.10 for RE = Tb. The molar ratio of EDTA to metal ions (Y^{3+}+RE^{3+}) was fixed at 0.1 and a molar ratio of urea to metal ions of 37.5 was employed to ensure a constant particle size for each of the phosphors synthesized.

The as-produced powders were fired for 3 h in air at various temperatures ranging from 950 to 1100 °C. Scanning electron microscopy (SEM) analysis using a Hitachi-S900 (2 kV accelerating voltage) was performed on the as-produced and fired samples, which where mounted directly to the imaging stub using conductive carbon tape. Transmission electron microscopy (TEM) was performed on fired samples using a JEOL 2000FX TEM operated at 200 kV. Nanophosphors were dispersed in acetone (0.1 mg/mL), sonicated for 10 min and cast onto a carbon-coated TEM grid.

The photoluminescence and radioluminescence intensities of the nanophosphors were measured from thin films spray-deposited onto quartz slides from a dilute acetone solution containing 1%:99% (w/w) polymethylmethacrylate to Y_2O_3:RE^{3+} using an airbrush. The photoluminescence (PL) of the nanophosphors were measured using a Jobin Yvon Horiba Raman Spectrometer with a 488 nm laser excitation wavelength. The same instrument was used to measure the RL of the highest-efficiency Y_2O_3:Eu^{3+} sample under excitation with a ^{210}Po 0.14 mCi/cm^2 alpha particle source. To acquire high-resolution spectra, the phosphors were exposed to the alpha-particle irradiation for ~3 min; a measurable decrease in RL intensity due to radiation-induced defects was observed to occur after weeks of exposure. An Ocean Optics HR2000 calibrated spectral radiometer was employed to measure the absolute RL power output from the samples under the same alpha particle source. X-ray diffraction (XRD) measurements were made on the spray-deposited samples using a Philips XpertPro powder X-ray diffractometer. The Cu$K\alpha$ line was used in the experiment with a scanning rate of 1.2°/min.

3. Results and discussion

3.1. Structural characterization

Fig. 1 contains representative SEM images of the Y_2O_3:RE^{3+} nanophosphors (a) pre- and (b) post-firing in air at 1100 °C for 3 h. Spherical particles were obtained with an average particle diameter 240±20 nm. Thermogravimetric analysis of the Y_2O_3:Eu^{3+} nanophosphor material showed two main first derivative decomposition peaks occurring at 170 and 620 °C, and no further weight loss after 750 °C. This is consistent with previous work in which the predominately amorphous material undergoes two decomposition reactions wherein H_2O and CO_2 are first lost at 180 °C, followed by the loss of an additional CO_2 at ~630 °C [17]. Firing the sample in air results in a material with a reduced average particle size of 200±20 nm. The total mass loss was approximately 40%, which is consistent with the theoretical hydroxycarbonate product weight loss of 38%.

XRD spectra were measured for a 5% doped Y_2O_3:Eu^{3+} sample fired at various temperatures as shown in Fig. 2. All of the firing temperatures yield highly crystalline cubic Y_2O_3 with an Ia3(206) space group, which is a stable lattice structure from room temperature to about 2600 K [18]. The Miller indices of the Bragg peaks are labeled in the figure (based on ICDD PDF-4 database

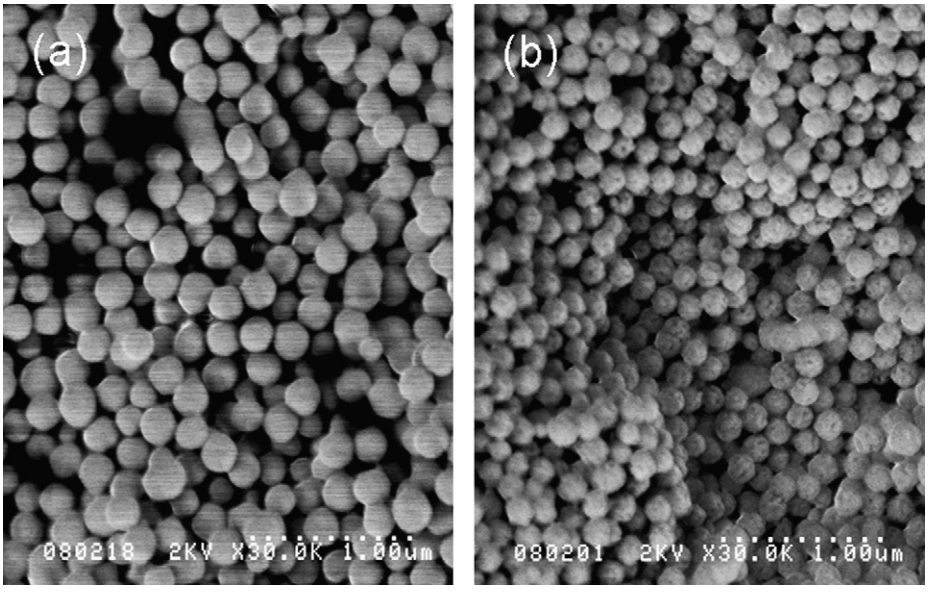

Fig. 1. Representative SEM images of Y_2O_3:RE^{3+} nanophosphors (a) pre- and (b) post-firing in air at 1100 °C for 3 h.

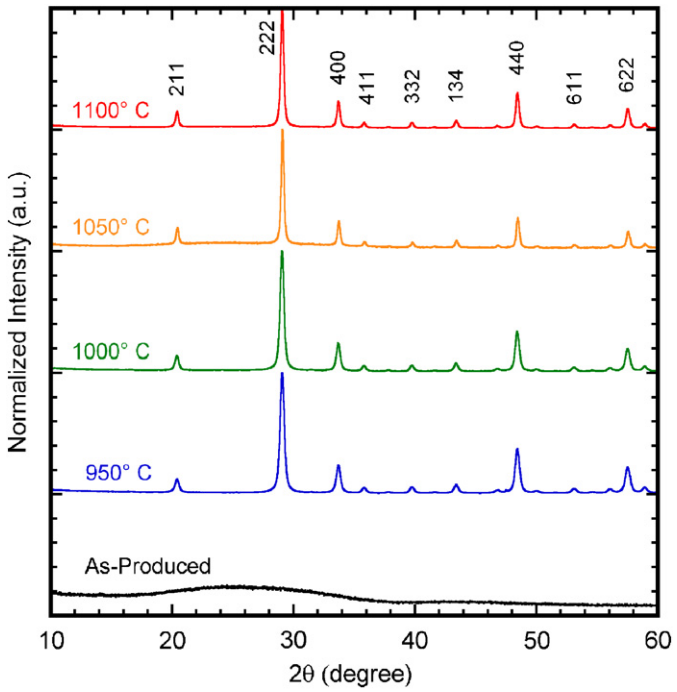

Fig. 2. X-ray diffraction spectra of the as-produced Y_2O_3:Eu^{3+} powder and after firing for 3 h at the temperatures listed. The prominent Bragg peaks have been labeled according to their corresponding lattice plane for cubic Y_2O_3.

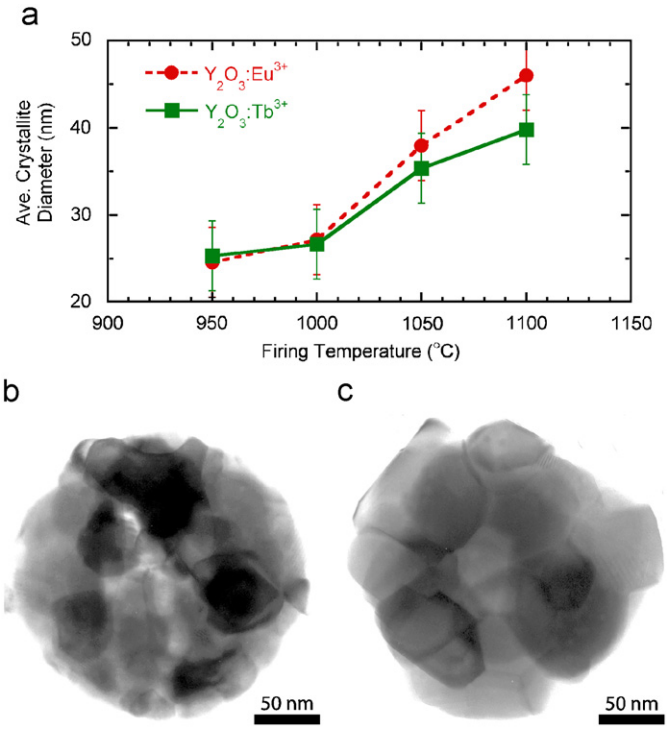

Fig. 3. (a) Calculated crystallite diameter variation with firing temperature based on Eq. (1) for 5% doped Y_2O_3:Eu^{3+} and 0.5% doped Y_2O_3:Tb^{3+}. (b) TEM image of the Y_2O_3:Eu^{3+} sample post-annealing at 950 °C for 3 h, and (c) post-annealing at 1100 °C for 3 h.

card no. 00-043-1036RDB). Similar trends were obtained when this procedure was performed on a 0.5% doped Y_2O_3:Tb^{3+} sample.

Analysis of the X-ray line broadening was performed to investigate the crystallite size and the residual strain within the particles using the Williamson–Hall relation [19]:

$$\beta = \frac{\lambda}{D\cos\theta} + 4\varepsilon\tan\theta, \quad (1)$$

where β is the full width at half maximum (FWHM) in radians, λ the X-ray wavelength (1.541 Å), D the crystallite diameter, θ the Bragg angle of the diffraction peak in radians, and ε the lattice distortion due to residual strain. The first term in Eq. (1) is the Scherrer formula, while the second term is the Stokes-Wilson formula and represents the broadening due to strain. A plot of $\beta\cos\theta/\lambda$ vs. $\sin\theta/\lambda$ using the FWHM of three different peaks with even–even–even Miller indices ((222), (440), and (622)) allows the crystallite diameter and residual strain to be estimated. From the analysis, the strain is relatively independent of firing temperature maintaining a value of $0.1\pm0.05\%$ for both the Y_2O_3:Eu^{3+} and Y_2O_3:Tb^{3+} samples (the as-produced material was not included in this analysis). However, an increase in crystallite size with firing temperature was observed and is plotted in Fig. 3a. Both materials have ~25 nm crystallite diameters after firing at 950 °C, which increases to greater than 40 nm after firing at 1100 °C. As a result, the ~200 nm particles depicted in Fig. 1b are polycrystalline, containing roughly 35 grains on the order of 40 nm each. The TEM images depicted in Fig. 3 support this result wherein small crystalline grains are clearly apparent within the particle fired at 950 °C, which grow in size after firing at 1100 °C. Similar polycrystalline structures have been observed in Y_2O_3:Eu^{3+} materials fired at 1200 °C for 30 min where voids within the materials were observable under TEM analysis [20]. However, in the literature, annealing for a longer period of time (>8 h) at 1050 °C has been shown to yield one large grain and may be a consideration for future optimization of the RL efficiency of Y_2O_3:RE^{3+} materials [20].

3.2. Optical characterization

A high degree of crystallinity is a critical phosphor characteristic, and is necessary for high PL and RL yield [10]. To assess the quality of the nanophosphors synthesized in the present work, high-resolution PL spectra of 5% Eu^{3+}-doped and 0.5% Tb^{3+}-doped Y_2O_3 nanophosphors (annealed at 1100 °C for 3 h) were measured (see Fig. 4). These samples had the highest intensity PL and RL and representative emission spectra for their respective dopants. The ability to vary the primary emission wavelength of Y_2O_3 simply by incorporating different dopants is exemplified in this figure. The tendency to favor radiative transitions over non-radiative transitions is made possible by the low energies (i.e., <100 meV) of the dominate phonon modes of the Y_2O_3 lattice [12]. Five characteristic Y_2O_3:Tb^{3+} emission peaks corresponding to the electronic transitions from the $^5D_4$ state to the ^7F_J ($J=2$–6) state of the Tb^{3+} ion are labeled [21] Likewise, the $^5D_0$–^7F_J ($J=0$–4) electronic transitions of the Eu^{3+} ion are labeled for the Y_2O_3:Eu^{3+} nanophosphor [13].

For comparison, the high-resolution RL spectra of the 5% doped Y_2O_3:Eu^{3+} is overlaid at the bottom of Fig. 4. Based on a SRIM-2003 simulation, the linear energy transfer by alpha-particles within Y_2O_3-based phosphors is on the order of a few hundred eV/nm [22,23]. Consequently, the number of excited electrons generated by each alpha-particle is drastically different than when excited by photons. It has been suggested that a high excitation rate can cause unwanted saturation effects in Y_2O_3-based phosphors leading to lower than expected light output [24]. Saturation results from the depletion of available activator sites caused by the high, localized excitation of alpha-particles [25]. This process may be characterized by a fast and a slow time constant: the former results from the initial electron and hole recombination at an activator, and the latter is due to delayed recombination at the same activators [26]. This delayed decay of

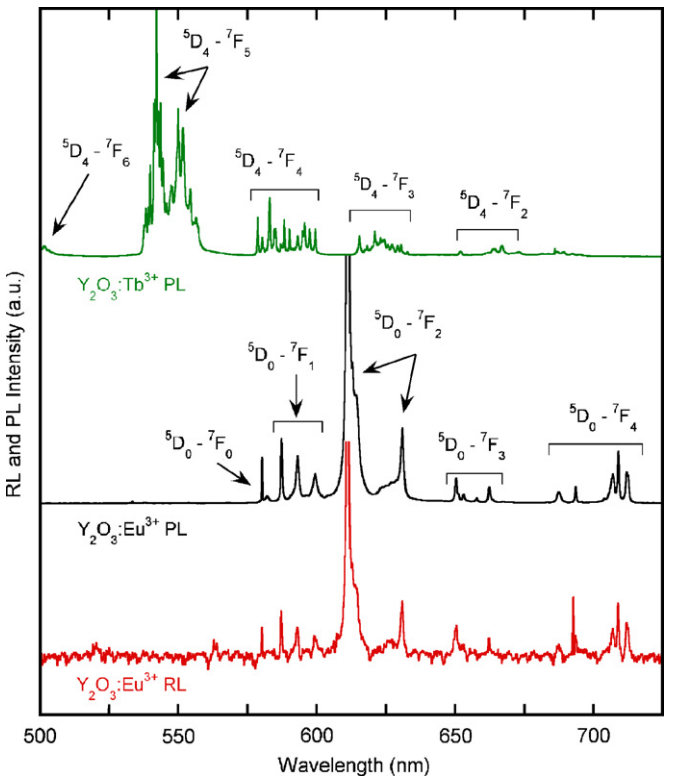

Fig. 4. The photoluminescence spectra of 0.5% Tb Y_2O_3 (top curve) and 5% Eu-doped Y_2O_3 (middle curve) under 488 nm photo-excitation and the radioluminescence spectrum of the latter (bottom curve) under a 0.14 mCi/cm^2 ^{210}Po alpha particle source (held at a distance of 2 mm). Both samples were fired at 1100 °C. The peak maximum (at 543 and 611 nm) has been scaled out of all curves to improve the clarity of the lower intensity transitions.

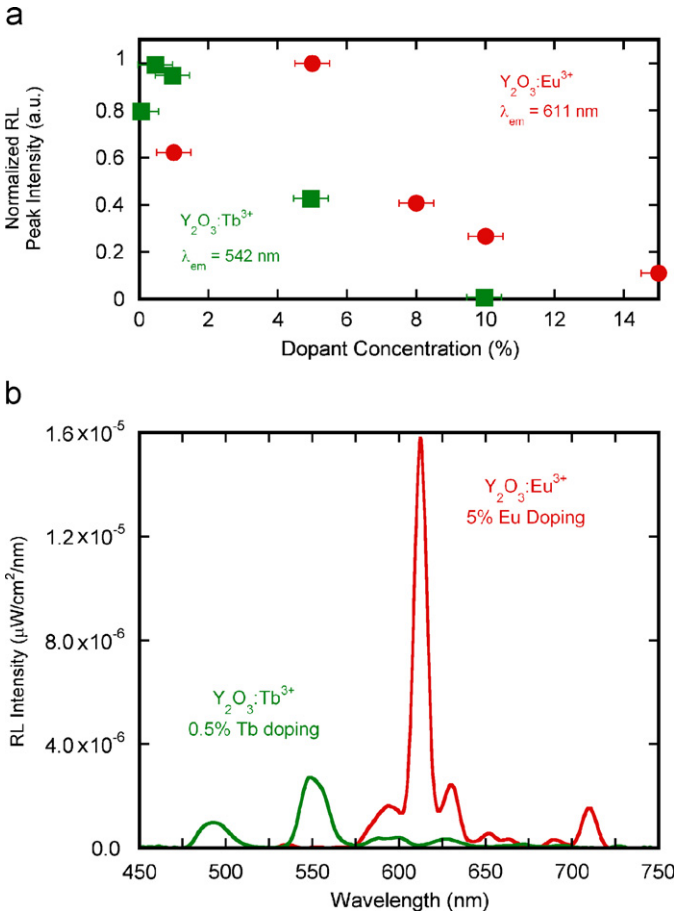

Fig. 5. (a) Normalized radioluminescence efficiency of the Y_2O_3:Tb^{3+} and Y_2O_3:Eu^{3+} for various concentrations of rare-earth ion dopant. (b) Radioluminescence spectra of 0.5% Tb^{3+} Y_2O_3 and 5% Eu^{3+} Y_2O_3 under excitation by a 0.14 mCi/cm^2 (circular area of ~2.5 cm^2) ^{210}Po source. The instrumental error is 10^{-8} μW/(cm^2 nm).

excited states associated with the activator ions may increase the probability of cross-relaxation between activator ions resulting in the population of the higher energy levels of one of activator ions. Therefore, emissions from higher energy levels should be observable provided the inter-activator distance is within a critical threshold. In comparing the Y_2O_3:Eu^{3+} PL and RL spectra, the $^5D_0$–^7F_J ($J = 0$–4) transitions do not appear to be effected by the high alpha-particle ionization rate. Furthermore, no significant peaks in the 525–568 nm range corresponding to higher $^5D_1$–^7F_J ($J = 0$–3) transitions or in the 500–520 nm range corresponding to the overlapping $^5D_2$–^7F_J and $^5D_3$–^7F_J transitions become visible. Although it is possible that emission from these transitions is below the detectable limit of our spectrometer, they represent a negligible contribution to the relaxation process of this material under alpha-particle excitation.

Based on the high-resolution PL and RL measurements, it is apparent that highly crystalline material was obtained. In fact, when held ~2 mm from a 0.14 mCi/cm^2 (circular area of ~2.5 cm^2) ^{210}Po alpha particle source (emitting 4.2 MeV alphas at a distance of 2 in, based on manufacturer specifications; NRD Inc.), green and red radioluminescence emission is visible with the naked eye (after only a few seconds of acclimation in a dark room) from the spray-deposited Tb^{3+} and Eu^{3+}-doped nanophosphors films, respectively. Fig. 5a depicts the normalized peak RL intensity of the Y_2O_3:Tb^{3+} and Y_2O_3:Eu^{3+} for various concentrations of rare-earth ion dopant. A total of nine measurements were made for each dopant concentration. Achieving the optimal doping level consists of a tradeoff between the number of emission sites and the formation of unwanted phases and lattice strain, which cause an increase in defects and thus the rate of non-radiative recombination. Reports of the optimal doping concentration for Y_2O_3:Tb^{3+} range from 0.5% to 2%, and vary depending on synthesis procedure, particle size, and excitation source (PL vs. cathodoluminescence) [27]. Similarly, the reported optimal Y_2O_3:Eu^{3+} doping concentration vary between 3% and 8% [11,28,29]. The optimal doping for the nanophosphors reported here measured under alpha-particle excitations are consistent with these reports.

The absolute RL intensity of the 0.5% doped Y_2O_3:Tb^{3+} and the 5% Y_2O_3:Eu^{3+} are overlaid in Fig. 5b. The higher RL intensity observed from the Y_2O_3:Eu^{3+} nanophosphor may be related to the higher doping concentration achieved prior to luminescence quenching. Y_2O_3:Tb^{3+} nanophosphors have been reported to accept a higher concentrations of Tb^{3+} ion over their bulk counter part (i.e., 1.5% vs. 0.5%), and therefore nanophosphors may have the potential to yield higher RL efficiencies [27,30]. However, it has yet to be confirmed whether the higher doping levels are an inherent nanomaterial/quantum effect or if the increased doping simply resulted in a larger concentration of non-photoactive impurities.

The demonstrated RL from Y_2O_3-based nanophosphors using two dopants is a critical first step towards realizing an indirect radioisotope battery. For instance, the peak emission of the Y_2O_3:Eu^{3+} nanophosphor material at 610 nm is well suited for conversion by an $InGaP_2$ photovoltaic device as it has a bandgap of 1.85 eV and a peak spectral responsivity in the 600–620 nm range (see Fig. 6). Likewise, a GaP (bandgap = 2.26 eV)-based photovoltaic device would be well matched to the 543 nm emission of the Y_2O_3:Tb^{3+} nanophosphor. (It should be noted that an ideal

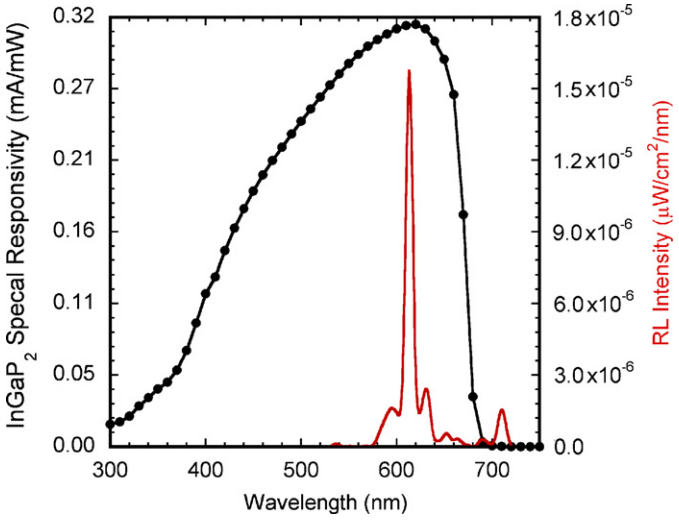

Fig. 6. Spectral responsivity of an $InGaP_2$ diode overlaid with the radioluminescence of the 5% Eu-doped Y_2O_3 nanophosphor. Details of the $InGaP_2$ device fabrication can be found in Ref. [1].

tuning of the phosphors RL would consist of a monochromatic emission at the peak responsivity of the photovoltaic converter.) Increased crystallinity and doping concentrations are the two measures investigated here for improving the radioluminescence yield from Y_2O_3-based nanophosphors. Co-doping may be an additional means for improving the RL efficiency of Y_2O_3-based phosphors. Such a scheme would rely on a one-way charge transfer mechanism between unalike neighboring dopant ions thereby increasing the level of excitation necessary for unwanted RL saturation and resulting in a higher effective total doping concentration.

4. Conclusion

Y_2O_3:Tb^{3+} and Y_2O_3:Eu^{3+} nanophosphors have been synthesized by the urea homogeneous precipitation method. The 200 nm particles were investigated using SEM, TEM, and XRD and indicated that a polycrystalline material was synthesized with an average crystallite size of ~40 nm after annealing for 3 h at 1100 °C. A comparison between the high-resolution RL and PL spectra did not reveal saturation effects caused by the high ionization rate of the alpha-particles. The radioluminescence intensity as a function of rare-earth ion doping concentration was shown to have a similar quenching curve to those reported in the literature for phosphors excited by photons or electrons, for both dopant species. The absolute radioluminescent intensity of a 5% Eu-doped Y_2O_3 nanophosphor was greater than that of the highest intensity Y_2O_3:Tb^{3+} phosphor which may be related to the higher activator concentration in the Eu^{3+}-based material. The coupling of a Y_2O_3:Eu^{3+} nanophosphor material with an $InGaP_2$ photovoltaic device is well suited for prospective indirect-conversion radioisotope batteries.

Acknowledgments

The authors would like to thank Professor Richard Hailstone and the RIT NanoImaging laboratory for the TEM analysis, and Christopher Schauerman for his assistance with phosphor synthesis. This work was supported in part by the DOD. Additionally, C.D.C. would like to acknowledge funding by NASA under a GSRP fellowship award no. NNX07AR57H.

References

[1] C.D. Cress, B.J. Landi, D.M. Wilt, R.P. Raffaelle, J. Appl. Phys. 100 (2006), 114519 (114511–114515).
[2] K.E. Bower, Y.A. Barbanel, Y.G. Shreter, G.W. Bohnert, Polymers, Phosphors, and Voltaics for Radioisotope Microbatteries, vol. 1, CRC Press, Boca Raton, FL, 2002.
[3] S.G. Bailey, D.M. Wilt, S.L. Castro, C.D. Cress, R.P. Raffaelle, Proc. IEEE PVSC 31 (2005) 106–109.
[4] J.H. Coleman, Nucleonics 11 (1953) 42–45.
[5] H. Li, A. Lal, J. Blanchard, D. Henderson, J. Appl. Phys. 92 (2002) 1122–1127.
[6] W.G. Pfann, Q.v. Roosbroeck, J. Appl. Phys. 25 (1954) 1422–1434.
[7] G. Rybicki, C. Vargas-Aburto, R. Uribe, Silicon carbide alphavoltaic battery, in: Proceedings of the 25th Photovoltaic Specialists Conference, 1996.
[8] W. Sun, N.P. Kherani, K.D. Hirschman, L.L. Gadeken, P.M. Fauchet, Adv. Mater. 17 (2005) 1230–1233.
[9] C.D. Cress, B.J. Landi, R.P. Raffaelle, Trans. Nucl. Sci. 55 (2008) to be published.
[10] S. Shionoya, W.M. Yen, Phosphor Handbook, 2, vol. 1, CRC Press, Boca Raton, FL, 1999.
[11] S.L. Jones, D. Kumar, K.-G. Cho, R. Singh, P.H. Holloway, Displays 19 (1999) 151–167.
[12] R. Schmechel, M. Kennedy, H.v. Seggern, H. Winkler, M. Kolbe, R.A. Fischer, L. Xaomao, A. Benker, M. Winterer, H. Hahn, J. Appl. Phys. 89 (2001) 1679–1686.
[13] J. Silver, M.I. Martinez-Rubio, T.G. Ireland, G.R. Fern, R. Withnall, J. Phys. Chem. B 105 (2001) 9107–9112.
[14] J. Silver, M.I. Martinez-Rubio, T.G. Ireland, G.R. Fern, R. Withnall, J. Phys. Chem. B 105 (2001) 948–953.
[15] J. Silver, T.G. Ireland, R. Withnall, J. Electron. Chem. Soc. 151 (2004) H66–H68.
[16] D. Matsuura, Appl. Phys. Lett. 81 (2002) 4526–4528.
[17] H.S. Yoo, H.S. Jang, W.B. Im, J.H. Kang, D.Y. Jeon, J. Mater. Res. 22 (2007) 2017–2024.
[18] V. Swamy, H.J. Seifert, F. Aldinger, J. Alloys Compds. 269 (1998) 201–207.
[19] G.K. Williamson, W.H. Hall, Acta Metall. 1 (1953).
[20] X. Jing, T. Ireland, C. Gibbons, D.J. Barber, J. Silver, A. Vecht, G. Fern, P. Trowga, D.C. Mortonb, J. Electrochem. Soc. 146 (1999) 4654–4658.
[21] H. Song, J. Wang, J. Lumin. 118 (2006) 220–226.
[22] J.F. Ziegler, J.P. Biersack, U. Littmark, The Stopping and Range of Ions in Solids, vol. 1, Pergamon, New York, 1985.
[23] J.F. Ziegler, J. Appl. Phys./Rev. Appl. Phys. 85 (1999) 1249–1272.
[24] P. Rossi, D.K. Brice, C.H. Seager, F.D. McDaniel, G. Vizkelethy, B.L. Doyle, Beam Int. Mater. At. 219–220 (2004) 327–332.
[25] R.B. Murray, A. Meyer, Phys. Rev. 122 (1961) 815.
[26] M. Nikl, A. Vedda, M. Fasoli, I. Fontana, V.V. Laguta, E. Mihokova, J. Pejchal, J. Rosa, K. Nejezchleb, Phys. Rev. B (Condens. Matter Mater. Phys.) 76 (2007) 195121.
[27] L.G. Jacobsohn, B.L. Bennett, R.E. Muenchausen, J.F. Smith, D.W. Cooke, Radiat. Meas. 42 (2007) 675–678.
[28] Q. Pang, J. Shi, Y. Liu, D. Xing, M. Gong, N. Xu, Mater. Sci. Eng. B 103 (2003) 57–61.
[29] M.L. Pang, J. Lin, Z.Y. Cheng, J. Fu, R.B. Xing, S.B. Wang, Mater. Sci. Eng. B 100 (2003) 124–131.
[30] M.A. Flores-Gonzalez, G. Ledouxa, S. Rouxa, K. Lebboua, P. Perriatb, O. Tillementa, J. Solid State Chem. 178 (2005) 989–997.